Thermochromic Halide Perovskite Windows with Ideal Transition Temperatures

Bryan A. Rosales, Janghyun Kim, Vincent M. Wheeler, Laura E. Crowe, Kevin J. Prince, Mirzo Mirzokarimov, Tom Daligault, Adam Duell, Colin A. Wolden, Laura T. Schelhas, and Lance M. Wheeler*

Urban centers across the globe are responsible for a significant fraction of energy consumption and CO_2 emission. As urban centers continue to grow, the popularity of glass as cladding material in urban buildings is an alarming trend. Dynamic windows reduce heating and cooling loads in buildings by passive heating in cold seasons and mitigating solar heat gain in hot seasons. Here, reduced energy consumption in highly glazed buildings in a mesoscopic building energy model is demonstrated when thermochromic windows are employed. Savings are realized across eight disparate climate zones of the United States. The model is used to determine ideal critical transition temperatures of 20–27.5 °C for thermochromic windows based on metal halide perovskite materials. Ideal transition temperatures are realized experimentally in composite metal halide perovskite films composed of perovskite crystals and an adjacent reservoir phase. The transition temperature is controlled by cointercalating methanol, instead of water, with methylammonium iodide and tailoring the hydrogen-bonding chemistry of the reservoir phase. Thermochromic windows based on metal halide perovskites represent a clear opportunity to mitigate the effects of energy-hungry buildings.

B. A. Rosales, J. Kim, K. J. Prince, M. Mirzokarimov, T. Daligault,
A. Duell, C. A. Wolden, L. T. Schelhas, L. M. Wheeler
National Renewable Energy Laboratory
15013 Denver West Parkway, Golden, CO 80401, USA
E-mail: lance.wheeler@nrel.gov
V. M. Wheeler
2qV Technology Company
University of Wisconsin—Stout
712 Broadway Street South, Menomonie, Wisconsin 54751, USA
L. E. Crowe
Swift Solar
981 Bing St, San Carlos, CA 94070, USA
K. J. Prince, C. A. Wolden
Department Chemical and Biological Engineering
Colorado School of Mines
Golden, CO 80401, USA

The ORCID identification number(s) for the author(s) of this article can be found under https://doi.org/10.1002/aenm.202203331.

1. Introduction

Buildings account for over one-third of the world's final energy consumption and ≈28% of global CO_2 emissions, which increases to >40% when building-related construction is included.[1] Urban areas composed of high-rise buildings continue to gain population and are predicted to encompass 70% of the world's population by the middle of this century.[2] At the same time, urban skylines increasingly feature glass façades and the architectural trend across building sectors is toward more glass, despite it greatly underperforming their opaque cladding counterparts for building efficiency.[3]

New window technology must be developed and deployed to reconcile the significant impact buildings have on the environment with the architectural demand for more glazing. Low-emissivity (low-e) coating technology revolutionized window energy-efficiency in the 1980s by selectively absorbing or reflecting infrared (IR) wavelengths while maintaining high transmittance of visible light. However, roughly half of the sun's energy is in visible wavelengths. Smart or dynamic window technologies typically target the visible spectrum by dynamically responding to stimulus (light, heat, electric field, etc.) with a change in optical properties. The transition from a visibly absorbing or reflecting (colored) state to a visibly transparent (bleached) state is leveraged to control solar heat gain to either offset heating loads or decrease cooling loads. Electrochromic windows, which transition from bleached to colored states in response to an electric field, offer active control of solar heat gain and glare, but soft costs and installation issues that lead to long payback times have plagued widespread deployment.[4] Thermochromic windows passively respond to changes in temperature to transition optical states. The lack of electrical components bypasses integration and soft-cost issues and enables simpler retrofits and opportunities for widespread deployment.

Thermochromic materials must have an ideal critical transition temperature (T_C), fast transition kinetics, a narrow hysteresis width (defined as the difference between the temperatures needed to switch from bleached to colored and colored to bleached), and high solar modulation ability.[5] Thermochromic materials include liquid crystals[6] and leuco dyes,[7] but

vanadium dioxide has been established as the quintessential solid-state thermochromic material for building applications. It has been the focus of research for decades due its relatively low-temperature insulator-to-metal Mott transition.[8] Though low compared to most oxides, 68 °C is well above the ideal T_C for window applications. An ideal T_C has been suggested to range between 10 and 28 °C based on various reports in the previous decade that typically study simplified buildings and glazing systems (savings reported relative to single-pane windows) and in single climate locations.[5,9,10] Significant research has thus been put into reducing the T_C of VO_2 with success in reaching $T_C < 30$ °C by using nanostructuring or doping.[11] However, reducing T_C slows the transition kinetics by decreasing the thermodynamic driving force and results in a larger hysteresis width due to the nature of the first-order phase transformation of VO_2.

Metal halide perovskite (MHP) materials are a class of semiconductors that have captured the imagination of the materials science community in the last decade due their unmatched optoelectronic properties and scalable solution processibility.[12] Most research has centered on photovoltaics[13] due to their extraordinarily absorption coefficients in the visible and near infrared regions of the solar spectrum. The inherently low formation energy of MHPs[14] enables rapid transformation from highly absorbing phases to highly transparent ones, which leads to unmatched solar modulation ability. State transformation is induced using intercalation,[15] crystal phase transformation,[16] and nanoparticle precipitation.[17] Each mechanism has now been leveraged to produce thermochromic windows. Perhaps the most interesting feature of MHPs as thermochromic materials is the opportunity to combine chromism with photovoltaic energy generation[15a,16,18] to bypass the fundamental tradeoff between visible transmittance (VT) of a photovoltaic window and power generation.[19] However, ideal transition temperatures for MHP-based thermochromic windows are yet to be demonstrated.

In this work, we combined building energy modeling with detailed materials design of new MHP composite materials for next generation thermochromic windows. We employed a mesoscopic modeling method to investigate building energy savings across eight disparate climate zones of the United States and compare to a baseline of window configurations that meet or exceed current energy efficiency standards. We find thermochromic windows improve energy efficiency across all climate zones and reveal a narrow window for the ideal transition temperature between 20 and 27.5 °C, regardless of climate zone. Our modeling motivates our experimental work to decrease MHP T_C below current demonstration. Incorporation of polymers, chloride, and methanol into perovskite composite films introduces a hydrogen-bonding chemistry that enables control over MHP T_C. We demonstrate MHP films with T_C tunable down to <22 °C. The films exhibit high solar modulation ability and durability >200 colored-to-bleached cycles due to polymer-induced nanoporous morphology.

2. Results and Discussion

### 2.1. Mesoscale Modeling Determines Energy Savings and Ideal Transition Temperature (T_c)

We apply a mesoscopic building energy model to accurately estimate building energy use across the various climate zones

of the United States (**Figure 1**a).[20] Thermochromic window laminates based on MHPs are simulated using transfer matrix method (TMM) software (*PVwindow*).[21] The TMM code solves Maxwell's Equations for stacks of thin films, such as the perovskite layer (thickness on the order of optical wavelengths), adjacent to thick "incoherent" layers like glass and laminate polymers (e.g., polyvinyl butyral (PVB)). We design the optical properties of the thermochromic laminate to have a dramatic swing between a VT of 73% in the bleached state and 5% in the colored state (Figure 1b). The VT for each state was chosen to maximize VT in the bleached state within the necessary materials stack and to reach VT levels that minimize solar heat gain in the colored state. The layers that contribute to the low-emissivity coating (thin silver) are the greatest limitation to higher VT and result in a maximum VT of 73%. VT = 5% and 0.5% are achieved by taking the same materials stack as the transparent state and replacing $MA_4PbI_6 \cdot 2H_2O$ with $MAPbI_3$. Thicker $MAPbI_3$ layers result in lower VT. A thickness of 370 nm results in VT = 5%, whereas a thickness of 775 nm results in VT = 0.5%. 5% and 0.5% were chosen because they are above and below the threshold for "privacy" in smart windows, which is a desirable design criterion for different applications (Figure S1, Supporting Information). It is noteworthy that VT has many different names in the literature but is defined the same way (see the Experimental Section), including visible light transmittance, average visible transmittance, and luminous transmittance (T_{Lum}).

More conventional materials like VO_2, which exhibit a metal-to-insulator transition, can modulate the infrared regions of the spectrum. Visible wavelengths make up roughly 51% of the sun's energy, whereas the IR and ultraviolet constitute 46% and 3%, respectively. Visible wavelength modulation is critical for energy savings and occupant glare comfort. Here we design thermochromic insulating glass units (IGUs) with low-e layers to statically modulate solar heat gain in the IR with perovskite materials that dynamically modulate the visible portion of the spectrum.

A building-level energy analysis was performed using a physics-based building energy simulation tool (EnergyPlus[22] and OpenStudio[23] software platforms) by incorporating thermochromic IGUs into a highly glazed office building model. IGUs were produced by incorporating optical data of the thermochromic laminates produced from *PVwindow* into software developed by Lawrence Berkeley National Laboratory[24] to create input files with necessary thermal, thermochromic, and optical data for the building simulation tool. Double-pane and triple-pane IGUs are designed to meet ASHRAE 90.1-2019 standards[25] based on center-of-glass U-factor, VT, and solar heat gain coefficient (SHGC) (Figure 1c). Gas fill (air or argon) and optical properties of the panes of glass (VT, emissivity from low-e coatings) are varied to meet regional standards (Table S1 and Table S2, Supporting Information). The VT and SHGC of the simulated thermochromic laminates are higher (bleached) or lower (colored) than ASHRAE standard properties while maintaining constant thermal properties (e.g., U-factor). The arithmetic average of the bleached and colored VT and SHGC do satisfy the ASHRAE standard, as is accepted practice for thermochromic windows.

Typical meteorological year (TMY3) weather data,[26] which include realistic sequences of time-dependent weather
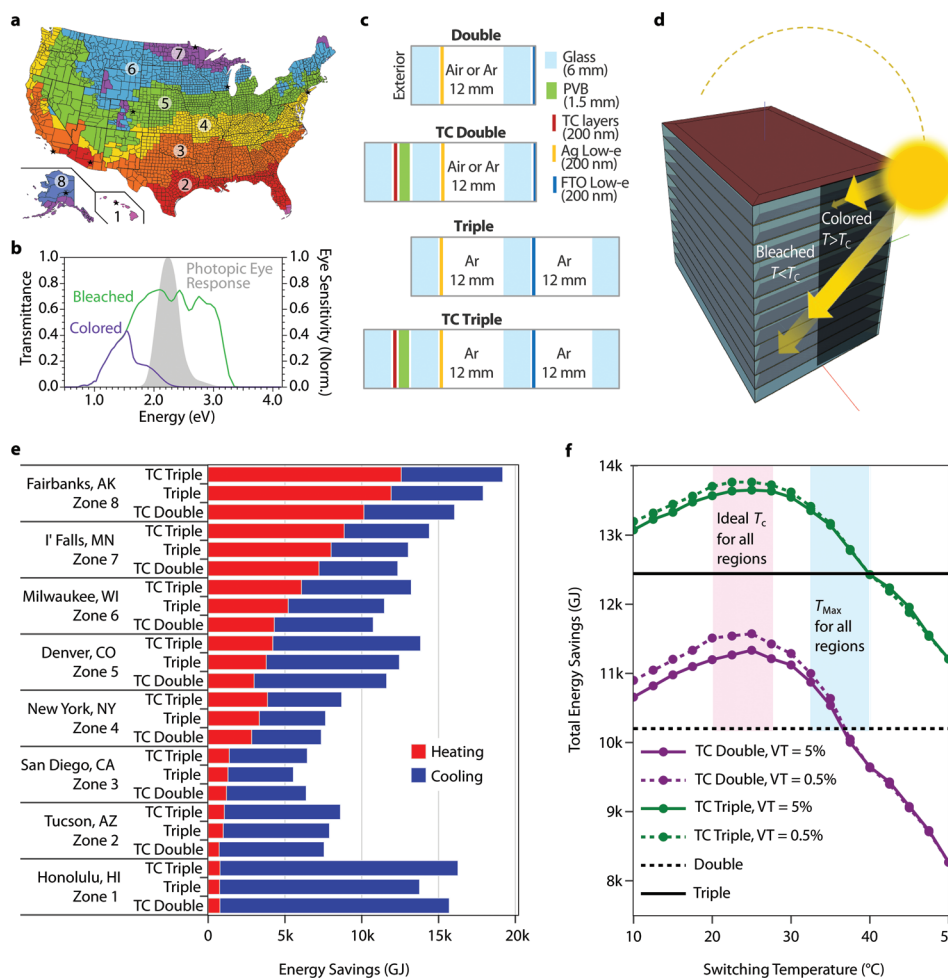
Figure 1. a) Representation of the eight climate zones in the United States, according to the International Energy Conservation Code. Each star on the map is a representative city in each zone where a building simulation was performed. b) Transmittance spectra produced by TMM calculation of the thermochromic laminate in colored and bleached states. The gray curve is the photopic eye response to highlight switching in the visible portion of the spectrum. c) Diagrams of insulating glazing units and d) highly glazed (95% window-to-wall ratio) 12-story medium office building used for mesoscale building energy analysis. The glass façade transitions from bleached to colored when the glass temperature is greater than the critical transition temperature (T_C). PVB = polyvinyl butyral. e) Annual energy savings due to heating (red) and cooling (blue) for eight United States climate zones with varied window construction. We define savings as the absolute difference between buildings with code-compliant glazing with thermochromic layers (TC double, triple-pane, or triple-pane glazing with thermochromic layers (TC Triple), and double-glazed windows. Cities are ordered from zone 8 (Fairbanks) at the top to zone 1 (Honolulu) at the bottom. f) Annual energy savings as a function of thermochromic window transition temperature for Denver, CO, USA. Shaded regions represent the range of ideal T_C (pink region) and maximum transition temperatures (T_{Max}, blue region) for cities in all climate zones. TC = thermochromic, VT = visible transmittance.

observations, are used against the building model to simulate various energy consumptions (e.g., heating, cooling, lighting, etc.) in the building in 15 min intervals. For instance, if the window transitions from bleached to colored during a 15 min interval, the model will adapt by increasing lighting in that region of the building to maintain comfortable lighting for the occupants. We study annual energy consumption for highly glazed buildings (window-to-wall ratio of 95%) in eight climate zones in the United States: Honolulu, HI; Tucson, AZ; San Diego, CA; Denver, CO; New York, NY; Milwaukee, WI; International Falls, MN; and Fairbanks, AK. The total primary energy use was calculated including both electricity and natural gas consumption. By coupling TMM simulation, which accommodate

nanoscopic optical effects, to large-scale building energy modeling, we employ bottom-up approach for evaluating window performance in buildings that spans nano-to-macro length scales. The window model relies solely only on the fundamental properties (complex refractive index) and thickness of the materials incorporated. This strategy enables detailed comparison of building performance based on optical switching without the influence of extraneous variables, a difficult task in experimental settings.

We simulated highly glazed office buildings to determine annual energy savings and ideal T_C of the perovskite-based thermochromic windows (Figure 1d). Relative to double-pane windows, thermochromic double-pane windows improve building

energy efficiency for each climate zone (Figure 1e). Energy savings are greater in colder regions (Milwaukee, International Falls, and Fairbanks) compared to hotter regions (Honolulu, Tucson, and San Diego). Thermochromic double-pane windows outperform even triple-pane windows in the hottest climate zones (Honolulu), despite their lower U-factors. In colder climates, triple-pane windows provide more energy savings than the thermochromic double-pane windows, but thermochromic triple-pane windows (triple-pane insulating glass unit where the outside pane is exchanged for a thermochromic laminate) provide the most annual energy savings compared to double-pane windows.

The source of improved energy efficiency in thermochromic windows, double or triple-pane, is modulation of heating and cooling loads in the building. In cooling dominated climates (Honolulu, Tucson, and San Diego), thermochromic windows reduce cooling load by mitigating solar heat gain (Figure 1e). Heating loads are also reduced in these cases, though less so. An analogous trend is observed for heating-dominated climates (Milwaukee, International Falls, and Fairbanks). Cooling loads notably decrease, but the reduction in heating load during the colder months shows a large benefit due to increased solar heat gain relative to double-pane windows that meet standards for the region, since the windows allow more solar heat gain while in the bleached state than low-e double-pane windows while still meeting ASHRAE standards. Climates with similar heating and cooling seasons (Denver and New York) benefit from reduced cooling and heating loads with thermochromic windows.

Greater impact in heating-dominated climates is perhaps counterintuitive since dynamic windows are often discussed as an effective technology to reduce solar heat gain.[5,9,10] However, most studies compare thermochromic window performance to single-pane glazing with no IR light mitigation (low-e layers) or with dynamic IR coatings like VO$_2$. Here, our baseline includes low-e layers since the perovskite materials only modulate visible wavelengths and it is a more meaningful comparison when choosing new-build or retrofit window options.

Our modeling studies show the significant heating savings potential of thermochromic windows. It is also worth noting thermochromic windows offer the distinct advantage of inexpensive retrofitting of storm windows. Retrofitting the existing building stock for energy efficiency is critical to reducing building energy use by 2050.[27] Our work suggests retrofitting a thermochromic laminate onto a single-pane or even double-pane window will yield significant savings. In addition to energy savings, dynamic windows also reduce glare to improve comfort. There is increasing evidence that office buildings with dynamic windows provide benefits to health, happiness, and productivity for their occupants.[28]

Maximum energy savings is determined by first calculating the thermochromic transition temperature that yields the highest energy savings in each climate zone. We define savings as the absolute difference between buildings with code-compliant glazing with thermochromic layers (TC double, triple-pane, or triple-pane glazing with thermochromic layers (TC Triple), and double-glazed windows with code-compliant low-e coatings that meet current standards for each region of

the United States. State-specific data, as reported by the Environmental Protection Agency,[29] are used to calculate primary energy use from site use. Thermal inputs are divided by total energy outputs to estimate the thermal efficiency of combustion-based electricity generation methods. Site energy use is multiplied by this value to estimate primary energy use.[20]
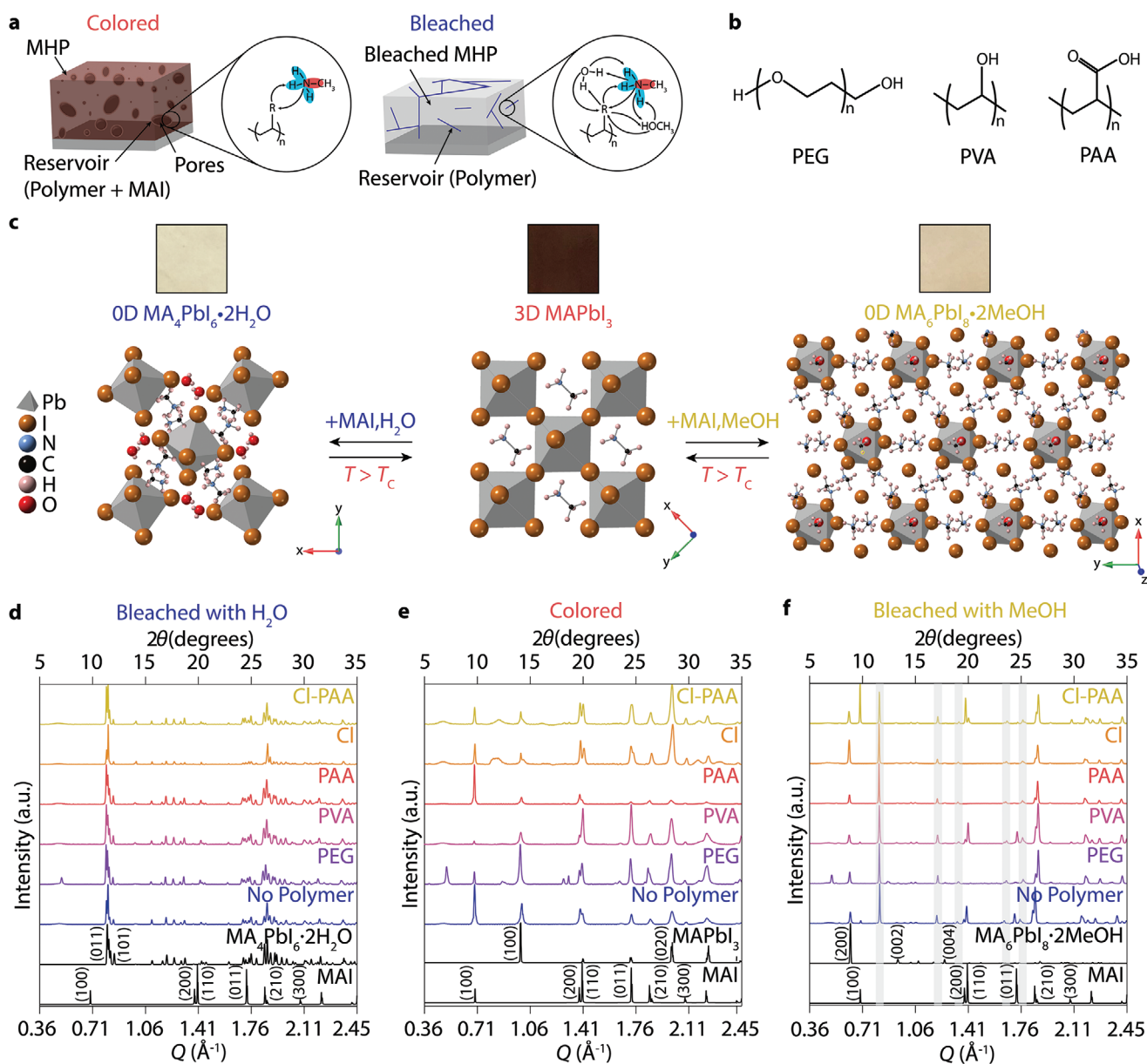
Each climate zone exhibits an ideal T_C, which maximizes energy savings as well as a maximum transition temperature (T_{Max}) that provides the same annual performance as code-compliant static windows (Figure 1e). Transition temperatures exceeding T_{Max} will reduce building efficiency—the building will consume more energy compared to having efficiency-standard-compliant double-pane windows. For example, the ideal T_C is 25 °C, and T_{Max} is 35 °C in Denver. Ideal T_C and T_{Max} do not vary significantly across climate zones, and the range is quite narrow. Ideal T_C is between 20 and 27.5 °C (pink shaded region, Figure 1f) and T_{Max} is between 32.5 and 40 °C (light blue shaded region, Figure 1f). Precise control of the thermochromic transition temperature to reach the ideal T_C is critical to successful deployment of thermochromic windows.

2.2. Additives Enable Control of MHP Critical Transition Temperature (T_C)

Previous work has demonstrated a tunable T_C of MHP materials to between 35 and 55 °C depending on the ambient humidity,[30] which is above the ideal switching temperature determined by the modeling described above. Here we tune T_C by formulating MHP-based composites that incorporate chloride and polymer additives into the film. (**Figure 2**a). We investigate poly(ethylene glycol) (PEG), poly(vinyl alcohol) (PVA), and polyacrylic acid (PAA), which have distinct functional groups that interact with components of the composite (Figure 2b). Switching is enabled by reversible transport of solvated salts to three-dimensionally connected lead halide lattice from a reservoir of excess methylammonium halide (MAX, where X = I⁻ or Cl⁻) (Figure 2c).[31]

Thermochromic composite MHP films were fabricated by spin-coating a solution of 4:1 methylammonium iodide (MAI):PbI$_2$ in N,N-dimethylformamide (DMF) onto glass followed by annealing at 100 °C for 10 min under inert conditions. Films containing Cl were fabricated by spin-coating a solution 6.5:1 MAI:PbCl$_2$ in DMF onto glass followed by annealing at 100 °C for 1 h under inert conditions. We incorporate polymers into MHP composite films by adding 1 molar equivalent of the polymer with respect to its monomer into the solutions described above (see the Experimental Section for more details).

The crystal structure of bleached and colored states of composite films are unaffected by the inclusion of polymer or chloride additives (Figures 2d–f). The colored films are brown and consist of two crystalline phases according to wide-angle X-ray scattering (WAXS): 1) (100) and (020) Bragg diffraction peaks of tetragonal MAPbI$_3$ and 2) the (100), (200), (110), (011), (210), and (300) Bragg diffraction peaks of crystalline MAI. Incorporation of polymers into the composite film does not introduce new diffraction peaks, except for additional crystalline peaks in the PEG composite MHP film at 0.50, 1.29, and 1.32 Å^{-1}. The relative intensity ratios of the MAI peaks change when polymers are

**ADVANCED
SCIENCE NEWS**

www.advancedsciencenews.com

**ADVANCED
ENERGY
MATERIALS**

www.advenergymat.de

Figure 2. a) Graphical illustration of composite MHP films in the colored and bleached states with insets illustrating the general molecular interactions present in both states. b) Structures of the polymers used in this study. c) Graphical illustration comparing the crystal structures of composite MHP films in the colored phase and upon exposure to H_2O and MeOH. Square insets in (c) are representative photographs comparing the color of each phase. d–f) Select wide-angle X-ray scattering (WAXS) data extracted from in situ cycling of composite MHP films exposed to H_2O/MeOH and 75 °C in Figures S2–S7 in the Supporting Information. Data were obtained from the last WAXS image of the first colored-to-bleached cycle. Gray bars in (f) indicate the additional phase associated with methanolation. The 2θ axes are relative to Cu K_α (1.5406 Å, 8.04 eV) radiation and was calculated from $Q = 4\pi\sin(\theta)/\lambda$ where λ is the excitation wavelength.

introduced, which we attribute to the incorporation of polymer into the "reservoir" of MAI that disrupts the crystal packing of the MAI molecules along different planes. In addition, no new peaks arise due to incorporation of chloride (the extra peak at 0.83 Å^{-1} is due to residual hydrated phases) because MACl is known to volatilize from MAPbI$_3$ films during annealing to leave a small amount of Cl in the film.[30] PAA decreases the relative intensity of the MAI when Cl is incorporated into composite film, which is consistent with PAA incorporation into the reservoir phase.

Bleached composite MHP films exhibit Bragg diffraction peaks that do not change with polymer or chloride additives, regardless of the intercalating solvent used (H_2O or MeOH). We conclude the mechanism of switching between bleached and colored states is not impacted by the additives (Figure 2d–f). Exposure to H_2O or MeOH vapor induces the disappearance of MAPbI$_3$ and MAI Bragg diffraction peaks with the emergence of (011) and (101) peaks characteristic of MA$_4$PbI$_6$•2H$_2$O (Figure 1d), the (200), (002), and (004) peaks characteristic of

$MA_6PbI_8 \cdot 2MeOH$ (Figure 2f), and additional peaks at 0.82, 1.21, 1.34, 1.65, and 1.78 Å^{-1} that are associated with methanolation (Figure 2f, gray boxes).[31] Bragg diffraction peaks characteristic of hydration and methanolation disappear when the composite MHP film is heated above T_C (Figure 2e). Some compositions show intermediate states between the distinct colored and bleached states, which correspond to mixed phase films. We attribute this to a dispersity in grain size within the film. The calculated Scherrer crystalline domain size suggests the film is composed of 39 ± 7 nm $MAPbI_3$ nanoparticles adjacent to a "reservoir" of MAI with a volume-averaged domain size of 50 ± 3 nm (Figure 2e).[32]

We determine T_C by heating bleached composite MHP films until a color change is observed. There are clear trends upon polymer and Cl incorporation with H_2O (**Figure 3**a) or MeOH (Figure 3b) used as the intercalating molecule. Exposure of composite MHP films to H_2O vapor at a concentration > 35% relative humidity (RH) bleaches the film due to the structural transformation of 3D $MAPbI_3$ to 0D $MA_4PbI_6 \cdot 2H_2O$ upon intercalation of $MAI \cdot H_2O$. Heating the film above the T_C of hydrated composite MHP films (70–75 °C, Figure 3c) reproduces the original brown color (Figure 3a) by dehydrating the film resulting in conversion of 0D $MA_4PbI_6 \cdot 2H_2O$ back into 3D $MAPbI_3$ (Figure 2e). Similarly, composite MHP films incorporating polymer bleach upon exposure to > 35% RH and then darken upon heating above T_C (Figure 3a). We find that T_C of hydrated composite MHP films follows the trend PEG (75–80 °C) > No Polymer (70–75 °C) > PVA (65–70 °C) > PAA (60–65 °C). Interestingly, even though incorporation of polymers affects T_C, they do not affect the time for bleaching to occur (t_{bleach}) upon hydration with all composite MHP films exhibiting t_{bleach} < 15 s (Figure 3d).

Exposing the same composite MHP films to MeOH vapor also bleaches the film (Figure 3b) due to the structural transformation of 3D $MAPbI_3$ into 0D $MA_6PbI_8 \cdot 2MeOH$ and the additional phase (Figure 2f) upon intercalation of $MAI \cdot MeOH$. Heating above the T_C of methanolated MHP films (45–50 °C, Figure 3c) reproduces the original brown color (Figure 3b) by demethanolating the film resulting in conversion of 0D $MA_6PbI_8 \cdot 2MeOH$ and the additional phase back into 3D $MAPbI_3$ (Figure 2f). We find that the T_C of all composite MHP films is reduced when MeOH is used as the switching molecule because MeOH exhibits weaker H-bonding compared to H_2O. Specifically, T_C of methanolated composite MHP films follows the trend PEG (65–70 °C) > PVA (55–60 °C) > No Polymer (45–50 °C) > PAA (40–45 °C). The hysteresis width was not determined, but we do not expect much deviation from similar chemistries presented in the literature (9.6–22.9 °C).[30] In contrast to hydration, t_{bleach} varies significantly upon methanolation following the trend PEG (120–130 s) > PVA (90–105 s) > No Polymer (75–90 s) ≅ PAA (75–90 s) (Figure 3d). The higher t_{bleach} of methanolation compared to hydration suggests the driving force for methanolation is weaker than hydration.

Incorporation of small amounts of Cl has been shown to reduce T_C.[30] Cl incorporation produces reddish films (Figure 3a and 3b) with a significantly blueshifted absorbance (Figure S8, Supporting Information). The films are bleached upon exposure to both H_2O and MeOH vapor with lower T_C values of 40–45 °C for hydrated films and 30–35 °C for methanolated

films (Figure 3c). The gradual loss of MACl during film formation also suggests that Cl is influencing the MHP film formation, and the Cl remaining in the film after annealing suggests that Cl may be facilitating transformations. Combining Cl-doping with the polymer exhibiting the lowest T_C, PAA, induces an even further drop in T_C to 30–35 °C for hydrated films and to 20–25 °C for methanolated films (Figure 3c). Cl and Cl-PAA also further reduce t_{bleach} upon methanolation to 60–75 s for both composite MHP films. Incorporation of polymers and Cl additives allow tunability of the T_C over a 50 °C window. MeOH allows control over t_{bleach} in a 60 s window, whereas H_2O-based composite films all switch within seconds. We successfully fabricate a composite MHP film exhibiting a T_C within the ideal window of 20–27.5 °C determined by building energy modeling through coincorporation of Cl with PAA and by using MeOH as the intercalation molecule. Our Cl-PAA films with MeOH exhibit our lowest T_C of 20–25 °C (Figure 3c) and our fastest t_{bleach} upon methanolation of 60–75 s (Figure 3d).

2.3. Tuning Switching Thermodynamics

We develop a simple thermodynamic model to describe the observed trends in transition temperature as a function of composite film chemistry. The colored-to-bleached transition occurs due to the intercalant (i), composed of solvated salts ($MAI \cdot MeOH$ or $MAI \cdot H_2O$), shuttling from an adjacent reservoir phase (R), composed of MAI, MeOH, or H_2O, and different polymers, into the $MAPbI_3$ crystal (C) to form a hydrated or methanolated phase (iC)
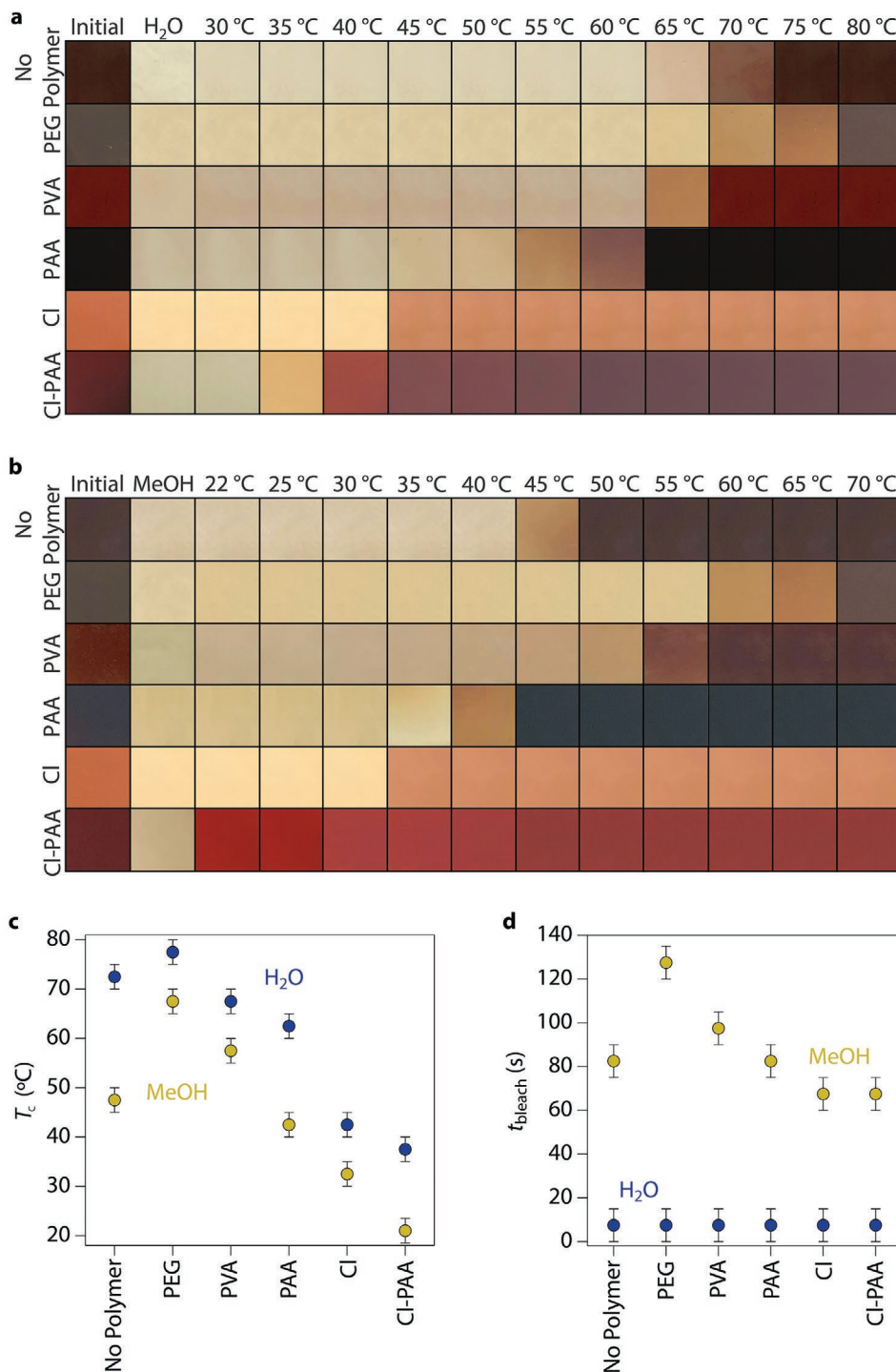
$$R + iC \rightleftharpoons iR + C \tag{1}$$

The film is bleached when the intercalant is thermodynamically favored in the crystal phase (left side of Equation (1)) and colored when the intercalant is favored in the reservoir phase (right side of Equation (1)). The equilibrium between the bleached state and the colored state is a function of temperature and the binding strength of the intercalant in each host (R and C). At room temperature, the intercalant is thermodynamically preferred in the crystal in all compositions except when PAA polymer and chloride additives are included and methanol is the solvent (Figure 3a,b).

A Gibbs' energy change of the reaction that is greater than zero ($\Delta G > 0$) will yield the bleached state, whereas $\Delta G < 0$ favors the colored phase

$$\Delta G = \Delta H - T\Delta S = \begin{cases} > 0, & \text{bleached} \\ < 0, & \text{colored} \end{cases} \tag{2}$$

where ΔH is enthalpy and ΔS is entropy of the system. Based on the observation of spontaneous reaction to the colored phase at higher temperatures, we conclude the bleached-to-colored reaction is an endothermic process where ΔH and ΔS are positive. ΔG will be negative to favor the colored phase when $T\Delta S > \Delta H$. (Equation (2)). The transition temperature (T_C) occurs when $\Delta G = 0$, so we have

$$T_C = \frac{\Delta H}{\Delta S} = \frac{H_{R+iC} - H_{iR+C}}{\Delta S} \tag{3}$$

**ADVANCED
SCIENCE NEWS**

www.advancedsciencenews.com

**ADVANCED
ENERGY
MATERIALS**

www.advenergymat.de

Figure 3. a,b) Photographs of composite MHP films incorporating polymers and/or doped with Cl showing color changes upon exposure to (a) H_2O and (b) MeOH followed by heating to 70 °C in 5 °C increments to identify the film's T_C. c) Thermochromic transition temperature (T_C) for each composite MHP film extracted from (a) and (b). d) Time for bleaching to occur (t_{bleach}) defined as the time for the MAPbI$_3$ (100) peak to disappear as determined from in situ WAXS data with a resolution of 15 s as shown in Figures S2–S7 in the Supporting Information.

The transition temperature is reduced by decreasing the difference in the enthalpy of the bleached state (H_{R+iC}) and colored state (H_{iR+C}) (Equation (3)). The effect of enthalpy change is visualized with a plot of ΔG as a function of temperature (**Figure 4**a). If we assume the entropy of the reaction is linear over a small temperature region and does not vary dramatically between different compositions, then the critical transition temperature is expected to decrease from $T_{C,1}$ to
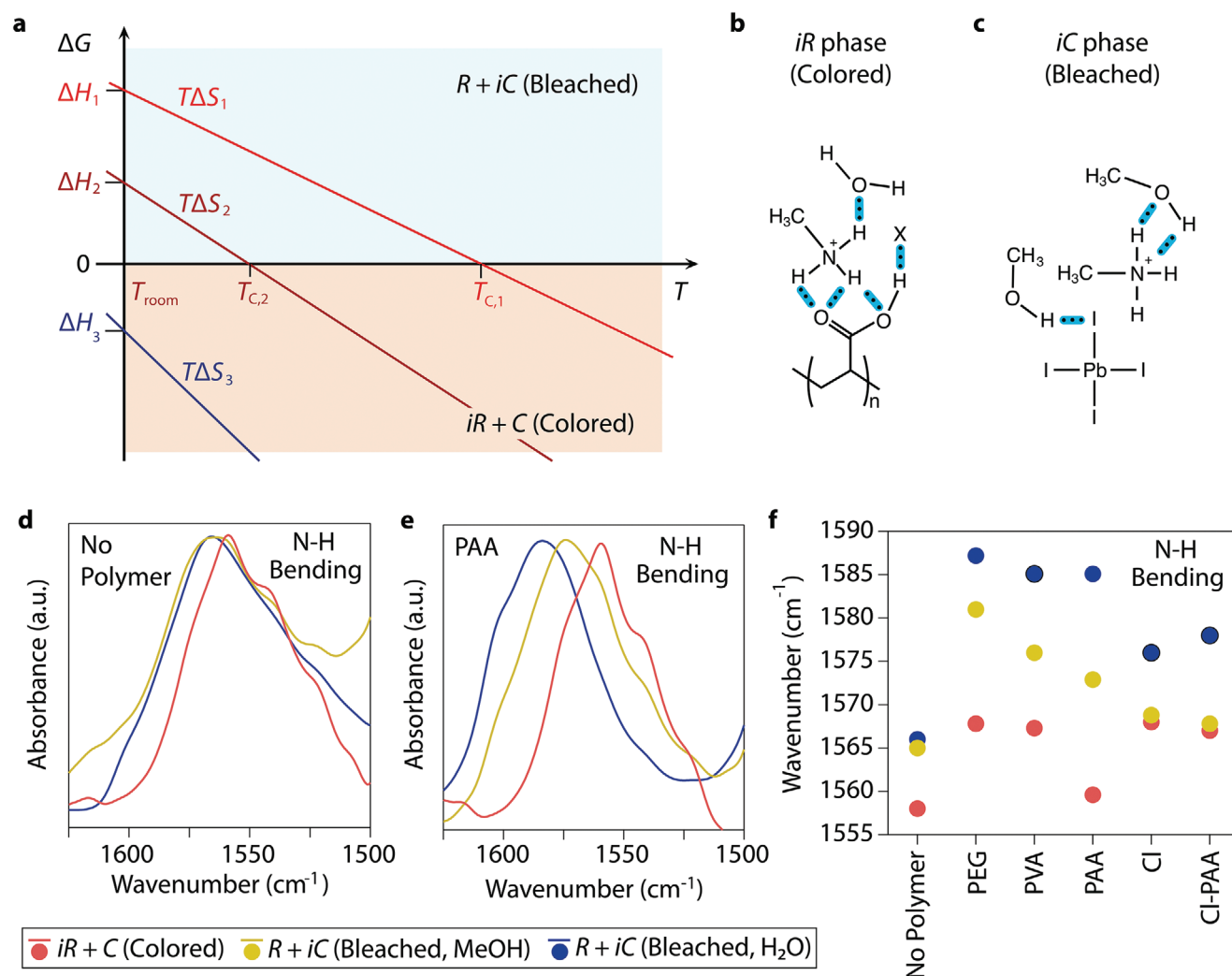
Figure 4. a) Gibbs' energy change as a function of temperature for three different composite MHP compositions showing control over transitions temperature (T_C). b,c) Illustrative examples of the different hydrogen bonds (blue highlights) that impact tuning ΔH. d,e) Attenuated total reflectance Fourier transform infrared (ATR-FTIR) spectra of the N−H bending mode of composite MHP films d) without polymer and e) including PAA in the colored state and after exposure to H$_2$O and MeOH. f) Peak position of the N−H bending vibrational modes for each composite MHP film in the colored state and after exposure to H$_2$O and MeOH.

$T_{C,2}$, when ΔH_1 is reduced to ΔH_2 (Figure 4a). If ΔH is further decreased to ΔH_3, then the colored phase is favored at any temperature above room temperature, and no transition occurs. ΔH is a function of the strength and number of bonds within the bleached and colored phases.[32] ΔH is decreased by decreasing H_{R+iC} or increasing H_{iR+C} (Equation (3)). There are ionic bonds that remain relatively constant in each of the compositions investigated here (e.g., Pb−I bonds). However, the number and strength of hydrogen bonds in the system is controlled by the choice of intercalating solvent (H$_2$O and MeOH), polymer, and chloride additives (Figure 4b,c).

We experimentally increase H_{iR+C} with the addition of a polymer with strong hydrogen bonding characteristics like the carboxylic acid groups of PAA (Figure 4b). Similarly, we decrease H_{R+iC} by swapping the intercalating solvent molecule from water to methanol since methanol does not form as many hydrogen bonds and weaker hydrogen bonds relative to water

(Figure 4c). Addition of PAA or using methanol leads to a decrease in ΔH (shift from ΔH_1 to ΔH_2 in Figure 4a). Adding chloride to the system changes ΔH to negative values since $H_{R+iC} < H_{iR+C}$, and the films remain colored at room temperature (ΔH_3 in Figure 4a).

H-bonding is critical to tuning T_C by changing ΔH. Attenuated total reflectance Fourier transform infrared spectroscopy (ATR-FTIR) allows us to probe H-bonding at the molecular level. ATR-FTIR spectra of films in the colored phase contain vibrational modes corresponding to methylammonium molecules in the reservoir and crystal, characterized by vibrational modes: N−H stretching between 2900 and 3250 cm^{-1}, N−H bending centered at 1557 cm^{-1}, N−H rocking centered at 1243 cm^{-1}, and C−N stretching centered at 970 cm^{-1} (Figure S9, Supporting Information).[33] Introduction of H$_2$O gives rise to characteristic O−H stretching, and introduction of MeOH exhibits C−H asymmetric stretching, C−H symmetric stretching, and C−O

stretching vibrational modes at 3440, 2970, 2830, and 1013 cm^{-1}, respectively (Figure S9, Supporting Information).[34]

The N−H bond of methylammonium halide molecules is a unique indicator of the H-bonding environment in both colored and bleached states (Figures 4b,c). Here we focus on the N−H bending mode due to its spectral isolation compared to other methylammonium bonds (Figure 4d.) When no polymer is incorporated into the composite MHP film, the N−H bending mode is centered at 1557 cm^{-1}. Upon exposure to H$_2$O or MeOH, the N−H mode shifts to higher energy, indicating a donation of electron density from the intercalating molecule to methylammonium, which is consistent with typical observations of bonding behavior between amines and hydroxyl groups. The N−H bending peak also broadens, which indicates a more chemically diverse bonding environment due to the presence of the intercalating species.

Polymers influence the N−H bonding environment in the composite MHP films. Addition of polymers to the composite films is confirmed by ATR-FTIR from the presence of vibrational modes characteristic of the functional groups of the polymers: C−O stretching of PEG at 1098 cm^{-1}, O−H stretching of PVA between 3550 and 3300 cm^{-1}, C=O and C−O stretching of PAA at 1710 and 1170 cm^{-1}, respectively. Exposure of the film to H$_2$O vapor causes characteristic O−H stretching vibrational modes to appear centered at 3490 cm^{-1} (Figure S9, Supporting Information).[35] The N−H bending mode signal is a convolution of MA molecules that are in the MHP crystal and those that are in the reservoir. The N−H bending mode is thus a measure of the influence of the polymers incorporated into the reservoir (Figure 4e). For PAA, the N−H bending mode in the colored state blueshifts slightly to 1560 cm^{-1} due to interactions with the carboxylic acid groups of the PAA. MAX•MeOH intercalation broadens and blueshifts the peak by donating and accepting H-bonds with the carboxylic acid groups and MeOH. H$_2$O further blueshifts the N−H bending peak due to more and stronger H-bonds formed.

The same general blueshifting trend is observed for PEG and PVA but to varying degrees (Figure 4f). Blueshifting of N−H vibrational modes is comparable between polymers with H$_2$O as the intercalation molecule, whereas blueshifting is increased according to PEG < PVA < PAA with MeOH as the intercalation species. The trend is consistent with the types of H-bonds provided by each polymer. The ether group of PEG will only donate electron density (accept H-bonds), which results in blueshifting of the N-H bond. In contrast, the acidic protons of in the hydroxyl and carboxylic acid groups of PVA and PAA, respectively, will accept and donate H-bonds. The ATR-FTIR signal of the N−H is a convolution of all H-bonds formed within the system, which results in a smaller overall shift due to also donating H-bonds to the polymer.

Though it is difficult to be quantitative, the trend in T_C between polymers is consistent with the polymer's ability to form H-bonds and effectively increase or decrease ΔH. PEG consistently increases T_C relative to the composite MHP film without polymers, and PEG is the weakest H-bonding polymer. PAA, on the other hand, consistently decreases T_C relative to other films. The carboxylic acid groups of PAA form the strongest and highest number of bonds compared to the others, which results in the lowest T_C. PVA is in between PEG

and PAA by decreasing T_C with H$_2$O and increasing T_C with MeOH relative to the composite MHP films without polymer. PVA's hydroxyl group is also capable accepting and donated H-bonds, though the bonds are weaker than those formed with carbonyl groups of carboxylic acid.[36]

Interestingly, the blueshift trend for methanolated compounds in the N−H bending mode (Figure 4f, yellow markers) follows the transition time trend quite well (Figure 3d). Kinetics are linked to our thermodynamic model though the rate constant. The rate constant is a function of the energy barrier height for the reaction. It is possible that increasing the hydrogen bond strength of the polymer in the reservoir phase also reduces the energy barrier between states. Further studies will be needed to validate the observation.

The influence of Cl$^-$ is not obvious from the N−H bond signal in ATR-FTIR. The N−H bending mode blueshifts in the presence of Cl$^-$ to a smaller degree than other samples. MACl likely only impacts film formation rather than ultimate film composition. However, MACl is highly hygroscopic, whereas MAI is not. Cl$^-$ is a hard Lewis base that will more readily accept H-bonds than I$^-$. Cl$^-$ will provide stronger H-bond interactions within the reservoir, which would have a similar impact as PAA and lead to increased H_{iR+C} and decreased T_C.

2.4. Nanoporous Morphology Improves Cyclability of Composite MHP Films

The polymers used in this study contain 11k–130k monomers connected in long chains with functional groups capable of H-bonding with the MAX reservoir. These long-chain polymers induce the formation of pores throughout the composite MHP film (**Figure 5**a, colored), and bleaching the film leads to a significant decrease in pore density (Figure 5a bleached). The overall thickness of the film is maintained within error during the transformation (colored 250 ± 20 nm; bleached 240 ± 7 nm), which suggests that any volume expansion that may result upon intercalation occurs within the void space of the pores rather than increasing the overall thickness of the film. Heating the film above T_C reforms the pores while maintaining the film thickness. These observations suggest that the polymers are likely located around the pores in the colored state and at grain boundaries in the bleached state (Figure 2a).

In addition to having a low T_C and rapid switching time, smart windows need to be durable. Cyclability of composite MHP films is currently limited by delamination and film reorganization upon repeated intercalation/deintercalation[15a] as well as deprotonation of MAI upon prolonged exposure to H$_2$O (Figure S10, Supporting Information). Polymers have been shown to impart mechanical stability in MHP films and can induce self-healing upon exposure to extreme mechanical stress.[37] Our composite MHP films containing polymer are porous with polymer located at the MHP/pore interface. Composite MHP films with this morphology should have improved mechanical stability to delamination and cracking.

We fabricated smart windows with composite MHP films containing PAA by sealing the film within two pieces of glass containing an atmosphere of N$_2$/MeOH with polyisobutylene (PIB) sealing the edges (Figure 5b). Smart windows with
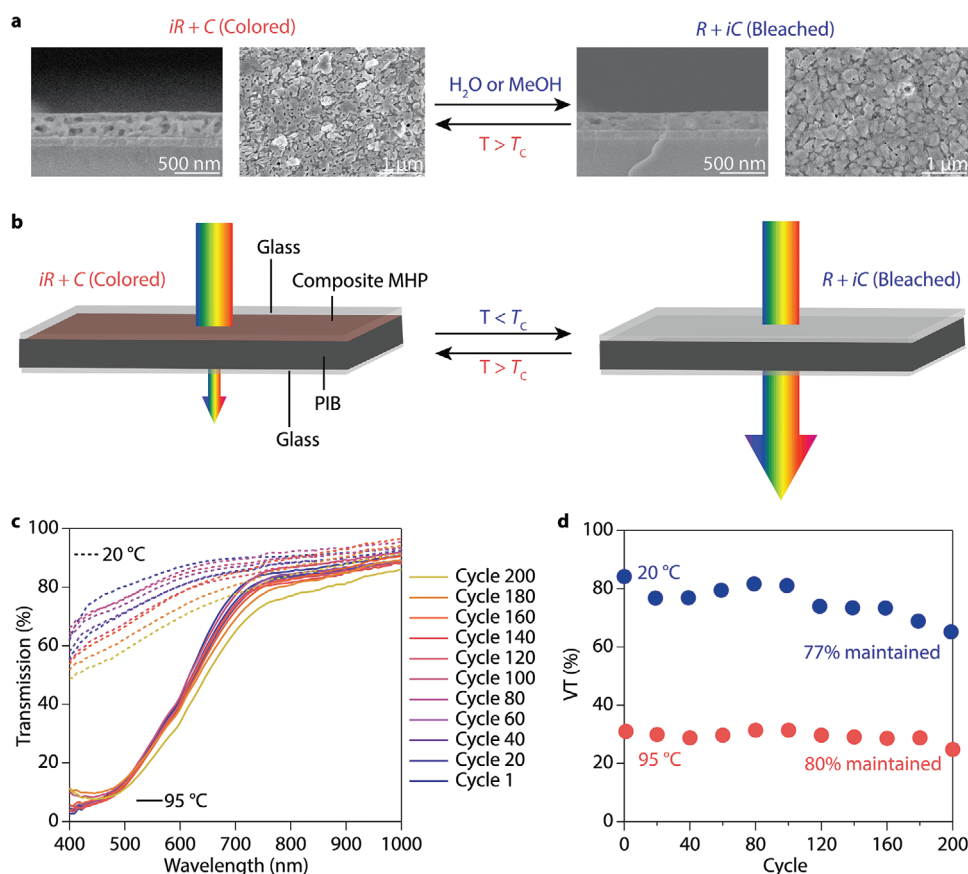
Figure 5. a) Representative scanning electron microscopy (SEM) images of composite MHP films containing polymer in the colored and bleached states. b) Illustration of composite MHP smart windows in the colored and bleached states. c) Transmittance and d) visible transmittance (VT) data over 200 thermochromic switching cycles of alternating exposure to 20 and 95 °C for a composite MHP film containing PAA and using MeOH as the intercalation molecule. 95 °C was chosen to increase the thermochromic switching speed.

this architecture become colored when heated above T_C and bleached when cooled below T_C. The VT of our smart windows cycle between 31% in the colored state and 84% in the bleached state (Figure 5c,d). Remarkably, our smart windows retain 77% of the initial VT in the bleached state and 80% in the colored state over 200 cycles. This result is the most cycles reported in thermochromic MHP films to date. The increasing baseline in the transmission spectra suggests the decrease in transmitted light after 200 cycles is largely due to increased haze (scattering) in the material. Increased scattering was observed in most compositions (Figure S10, Supporting Information) and will need to be improved for practical deployment.

3. Conclusion

In this work, we employed a mesoscopic building energy model to evaluate the energy savings and ideal thermochromic switching temperature of MHP-based windows. Our model indicates an increase in building performance across all climate zones. Thermochromic windows supplied a significant savings compared to windows that meet current standards. We showed the most savings in heating-dominated climates is due to passive solar heating in winter months. The model also allowed us

to determine the ideal thermochromic critical transition temperature, which exists in a tight range of 20–27.5 °C. We used the model to motivate our experimental work to tailor composite metal halide perovskite films to switch at lower temperatures than currently realized. We tuned switching in MHP films down to <22 °C by employing methanol as the intercalating solvent, including polyacrylic acid in the reservoir phase, and incorporating chloride anions into the composite. Films demonstrated durable thermochromic switching for 200 bleached-to-colored cycles. The work demonstrates the extraordinary promise of thermochromic metal halide perovskites to reduce building energy consumption and mitigate climate change without sacrificing the architectural freedom of glazing.

4. Experimental Section

Mesoscopic Building Energy Modeling: *PVwindow* software was used to simulate nanoscale stacks of materials that compose dynamic or photovoltaic (PV) glazing (github.com/NREL/PVwindow). The software solves Maxwell's equations for stacks of optically thin and thick materials to yield spectral absorptivity, reflectivity, and transmissivity at a chosen incident solar angle.[2] Simulated spectra are imported into OPTIC 6 software to input the files into the International Glazing Database. Files were imported into WINDOW 7 software to simulate insulating glass units and .IDF files were exported for importing into

Open Studio[23] for EnergyPlus[22] simulations by incorporating IGUs (installed on all cardinal directions) into the building model. A 12-story medium office building model with 95% window-to-wall ratio was created based on the Department of Energy (DOE) prototype building model[38] and all the remaining configurations (e.g., wall/roof insulation, equipment efficiency, occupancy schedule etc.) of the building followed the ASHRAE 90.1-2010 standards.[25] A typical meteorological year (TMY3) weather data,[26] which includes realistic sequences of time dependent weather observations, is used against the building model to simulate various energy consumptions (e.g., heating, cooling, lighting, etc.) in the building in every 15 min intervals and for a year.

Materials and Chemicals: PbI_2 (99.99%) was purchased from TCI Chemicals. MAI (99.99%) was purchased from Greatcell Solar Materials. N,N-dimethylformamide (DMF, 99.8%, anhydrous), $PbCl_2$ (99.999%), Al_2O_3 nanoparticles (<50 nm, 20 wt% in isopropyl alcohol (IPA)), poly(acrylic acid) (PAA, M_n = 130k), and PEG (M_n = 30k) were purchased from Sigma-Aldrich. PVA (98–99% hydrolyzed, M_w = 11k–31k) was purchased from Alfa Aesar. Methanol (MeOH) was purchased from Fisher. All chemicals were used as received.

Film Fabrication and Transition Temperature Determination: Thermochromic MHP films were fabricated by spinning a 0.2 –0.6 м solution containing 4:1 MAI: PbI_2 (No Polymer MHP film) or 4:1:1 MAI:PbI_2:polymer (PEG, PVA, PAA MHP films, molar mass of the polymer's monomer was used) in DMF on glass at 4000 rpm for 30 s followed by annealing at 100 °C for 10 min under N_2. Films containing Cl were fabricated by the same methods except a solution containing 6.5:1 MAI:$PbCl_2$ (Cl MHP film) or 6.5:1:1 MAI:$PbCl_2$:PAA (Cl-PAA MHP film) in DMF was used instead and annealing was performed at 100 °C for 1 h under N_2. H_2O vapor was introduced via a glovebox equipped with a humidity controller connected to a humidity sensor, commercial humidifier, and house compressed air as a dehumidifier. MeOH vapor was introduced by placing a composite MHP film into a container with liquid MeOH at the bottom until the MHP film turns transparent and colorless. Overexposure to MeOH causes the MHP film to turn opaque white with reduced thermochromic response. The thermochromic transition temperature (T_C) was measured by heating a bleached composite MHP film on a hotplate kept at < 15% RH at 5 °C intervals measured by an infrared thermometer gun until the composite MHP film transitions from colorless to a dark.

Structural and Morphological Characterization: In situ WAXS data were collected at the Stanford Synchrotron Radiation Light Source (SSRL) at beamline 11-3. The composite MHP film were measured at an incident angle of 3° and an incident X-ray wavelength of $\lambda_{synchrotron}$ = 0.9744 Å. A Rayonix MX225 2D detector was used to collect data and a LaB_6 standard used to calibrate the data. MeOH vapor was introduced to the sample chamber by flowing He through a bubbler containing MeOH via a Schlenk line. H_2O vapor was introduced to the sample chamber using a commercial room humidifier powered by a humidity controller, which was connected to a humidity sensor within the sample chamber. MeOH and H_2O vapor concentrations in the sample chamber were reduced by flowing helium gas through the chamber. Data acquisition was continuous except for brief interruptions for changing the sample chamber connection between MeOH, H_2O, and He. The integration time per measurement was 15 s. The data were integrated using GSASII.[39] Q and 2θ values were calculated by converting $2\theta_{synchrotron}$ to Q (Q = $4\pi \sin(2\theta/2)/\lambda_{synchrotron}$) and to $2\theta_{Cu\ K\alpha}$ ($2\theta_{Cu\ K\alpha}$ = $2*\arcsin(Q*\lambda_{Cu\ K\alpha}/4\pi)$) relative to Cu K_α (1.5406 Å, 8.04 eV). Scherrer analysis was performed using a κ value of 0.9 and full width at half maximum values with error bars obtained by fitting peaks to a Voigt function. Scanning electron microscopy (SEM) images were collected with a Hitachi S-4800 Field Emission SEM and MHP film was prepared on indium tin oxide substrates.

Optical Characterization: Absorbance of films and transmittance of smart windows was collected with an Ocean Optics Maya 2000 Pro UV–vis Spectrophotometer. Films were prepared as above except No Polymer and Cl MHP films were spun on a ≈400 nm thick mesoporous Al_2O_3 scaffold prepared by spinning a 5 wt% solution of Al_2O_3 NPs in IPA onto UV-ozoned glass at 3000 rpm for 30 s followed by annealing

at 500 °C for 30 min. All spectra were collected at 22 °C and substrate absorbance was subtracted from all spectra. Visible transmittance, or luminous transmittance, is determined by the number of photons transmitted through window, T, weighted by the sensitivity of the human eye to see those photons, which is defined as the photopic luminosity function, $\varphi = \varphi(E)$ [24]

$$VT = \frac{\int \Gamma\ T\ \varphi\ dE}{\int \Gamma \varphi\ dE} \quad (4)$$

The value is divided by the total incident intensity, Γ, weighted by φ and integrated over the total spectrum giving values between zero and one.

ATR-FTIR Measurements: A Bruker Alpha FTIR spectrometer outfitted with a diamond attenuated total reflection Fourier transform infrared (ATR-FTIR) spectroscopy attachment with heating and cooling capabilities was used in the study. Composite MHP films were made by drop-casting 1 µL of the above solutions with a concentration of 0.1 м (No Polymer and Cl films) or 0.05 м (PEG, PVA, PAA, Cl-PAA films) onto the ATR crystal. A custom glass chamber with an O-ring was placed over the ATR crystal stage to enclose the solution and connect the stage to a Schlenk line. The solution was annealed at 100 °C for 30 min under N_2 flow to ensure all DMF was evaporated prior to data acquisition. The film was bleached by flowing N_2 through a bubbler containing MeOH or H_2O at a rate of 1–3 bubbles s^{-1} at 25 °C. Flowing N_2 was used to purge the glass chamber encasing the film before data acquisition to ensure that only MeOH or H_2O within the film and not in the atmosphere was detected. MeOH or H_2O were removed from the film by heating the ATR stage to 100 °C and the stage was cooled back to 25 °C before data acquisition. The temperatures reported are those measured and delivered to the ATR stage with OPUS 7.2 software. All spectra were collected between 350 and 4000 cm^{-1} with a resolution of 2 cm^{-1} under N_2 flow.

Smart Window Fabrication: Thermochromic MHP films for smart windows were fabricated as described above with a 0.2 м solution containing 4:1:1 MAI:PbI_2:PAA in DMF. MHP on the outer 3 mm edge of the glass substrate was scraped off with a razor blade. A layer of PIB was placed on the clean edge, another glass substrate was placed on top and the glass layers were pressed together to form a seal. The atmosphere inside the smart window was replaced with N_2/MeOH or N_2/H_2O by poking a hole in the PIB, flowing N_2 through a bubbler containing MeOH or H_2O at a rate of 1–2 bubbles s^{-1} until the film transitions from colored to transparent colorless and then immediately plugging the hole with more PIB.

Supporting Information

Supporting Information is available from the Wiley Online Library or from the author.

Acknowledgements

Conflict of Interest

The authors declare no conflict of interest.

Data Availability Statement

The data that support the findings of this study are available from the corresponding author upon reasonable request.

[1] Tracking Buildings 2020, https://www.iea.org/reports/tracking-buildings-2020 (accessed: September 2021).

[2] R. K. Pachauri, L. A. Meyer, *Climate Change 2014: Synthesis Report*, IPCC, Geneva, Switzerland **2014**, p. 151.

[3] A. Wilson, *Green Build., Environ., Energy Civ. Eng., Proc. Int. Conf. Green Build., Mater. Civ. Eng.* **2010**, *19*, 19.

[4] D. R. Needell, M. E. Phelan, J. T. Hartlove, H. A. Atwater, *Energy* **2021**, *219*, 119567.

[5] M. Aburas, V. Soebarto, T. Williamson, R. Liang, H. Ebendorff-Heidepriem, Y. Wu, *Appl. Energy* **2019**, *255*, 113522.

[6] M. Seredyuk, A. B. Gaspar, V. Ksenofontov, S. Reiman, Y. Galyametdinov, W. Haase, E. Rentschler, P. Gütlich, *Chem. Mater.* **2006**, *18*, 2513.

[7] R. Kulčar, M. Friškovec, N. Hauptman, A. Vesel, M. K. Gunde, *Dyes Pigm.* **2010**, *86*, 271.

[8] T.-C. Chang, X. Cao, S.-H. Bao, S.-D. Ji, H.-J. Luo, P. Jin, *Adv. Manuf.* **2018**, *6*, 1.

[9] L. Long, H. Ye, *Sci. Rep.* **2014**, *4*, 6427.

[10] X. Hong, F. Shi, S. Wang, X. Yang, Y. Yang, *Build. Simul.* **2021**, *14*, 1685.

[11] M. E. A. Warwick, R. Binions, *J. Mater. Chem. A* **2014**, *2*, 3275.

[12] B. Dou, J. B. Whitaker, K. Bruening, D. T. Moore, L. M. Wheeler, J. Ryter, N. J. Breslin, J. J. Berry, S. M. Garner, F. S. Barnes, S. E. Shaheen, C. J. Tassone, K. Zhu, M. F. A. M. van Hest, *ACS Energy Lett.* **2018**, *3*, 2558.

[13] J. Y. Kim, J. W. Lee, H. S. Jung, H. Shin, N. G. Park, *Chem. Rev.* **2020**, *120*, 7867.

[14] B. A. Rosales, K. Schutt, J. J. Berry, L. M. Wheeler, (Preprint), arXiv:2209.13655, submitted Sep 2022.

[15] a) L. M. Wheeler, D. T. Moore, R. Ihly, N. J. Stanton, E. M. Miller, R. C. Tenent, J. L. Blackburn, N. R. Neale, *Nat. Commun.* **2017**, *8*, 1722; b) L. M. Wheeler, N. C. Anderson, T. S. Bliss, M. P. Hautzinger, N. R. Neale, *J. Phys. Chem. C* **2018**, *122*, 14029.

[16] J. Lin, M. Lai, L. Dou, C. S. Kley, H. Chen, F. Peng, J. Sun, D. Lu, S. A. Hawks, C. Xie, F. Cui, A. P. Alivisatos, D. T. Limmer, P. Yang, *Nat. Mater.* **2018**, *17*, 261.

[17] a) M. De Bastiani, M. I. Saidaminov, I. Dursun, L. Sinatra, W. Peng, U. Buttner, O. F. Mohammed, O. M. Bakr, *Chem. Mater.* **2017**, *29*, 3367; b) G. Vats, B. Hodges, A. J. Ferguson, L. M. Wheeler, J. L. Blackburn, *Adv. Mater.* **2022** https://doi.org/10.1002/adma.202205459.

[18] a) S. K. Sharma, C. Phadnis, T. K. Das, A. Kumar, B. Kavaipatti, A. Chowdhury, A. Yella, *Chem. Mater.* **2019**, *31*, 3111; b) A. Halder, D. Choudhury, S. Ghosh, A. S. Subbiah, S. K. Sarkar, *J. Phys. Chem. Lett.* **2015**, *6*, 3180.

[19] L. M. Wheeler, V. M. Wheeler, *ACS Energy Lett.* **2019**, *4*, 2130.

[20] V. M. Wheeler, J. Kim, T. Daligault, B. A. Rosales, C. Engtrakul, R. C. Tenent, L. M. Wheeler, *One Earth* **2022**, *5*, 1271.

[21] S. J. Byrnes, (Preprint), arXiv:1603.02720, submitted: March, 2016.

[22] D. B. Crawley, L. K. Lawrie, F. C. Winkelmann, W. F. Buhl, Y. J. Huang, C. O. Pedersen, R. K. Strand, R. J. Liesen, D. E. Fisher, M. J. Witte, J. Glazer, *Energy Build.* **2001**, *33*, 319.

[23] R. Guglielmetti, D. Macumber, N. Long, *OpenStudio: An Open Source Integrated Analysis Platform*, NREL, United States **2011** https://www.nrel.gov/docs/fy12osti/51836.pdf.

[24] D. C. Curcija, D. S. Vidanovic, R. G. Hart, C. J. Jonsson, R. D. Mitchell, LBNL Technical Report, April **2018**.

[25] ANSI/ASHRAE/IES Standard 90.1-2019, https://www.ashrae.org/technical-resources/bookstore/standard-90-1 (accessed: September 2021).

[26] EnergyPlus Weather Data, https://energyplus.net/weather (accessed: September 2021).

[27] B. Guneralp, Y. Zhou, D. Urge-Vorsatz, M. Gupta, S. Yu, P. L. Patel, M. Fragkias, X. Li, K. C. Seto, *Proc. Natl. Acad. Sci. U. S. A.* **2017**, *114*, 8945.

[28] A. Hedge, C. McKee, *Proceedings of the Human Factors and Ergonomics Society Annual Meeting* **2020**, *64*, 531.

[29] United States Environmental Protection Agency (EPA), 2022, "Emissions & Generation Resource Integrated Database (eGRID), 2020" Washington, DC: Office of Atmospheric Protection, Clean Air Markets Division, https://www.epa.gov/egrid.

[30] S. Liu, Y. W. Du, C. Y. Tso, H. H. Lee, R. Cheng, S. P. Feng, K. M. Yu, *Adv. Funct. Mater.* **2021**, *31*, 2010426.

[31] B. A. Rosales, L. E. Mundt, L. T. Schelhas, L. M. Wheeler, *J. Am. Chem. Soc.* **2022**, *144*, 667.

[32] B. A. Rosales, L. E. Mundt, T. G. Allen, D. T. Moore, K. J. Prince, C. A. Wolden, G. Rumbles, L. T. Schelhas, L. M. Wheeler, *Nat. Commun.* **2020**, *11*, 5234.

[33] G. Schuck, D. M. Többens, M. Koch-Müller, I. Efthimiopoulos, S. Schorr, *J. Phys. Chem. C* **2018**, *122*, 5227.

[34] I. Doroshenko, V. Pogorelov, V. Sablinskas, *Dataset Pap. Chem.* **2013**, *2013*, 329406.

[35] V. M. Wallace, N. R. Dhumal, F. M. Zehentbauer, H. J. Kim, J. Kiefer, *J. Phys. Chem. B* **2015**, *119*, 14780.

[36] G. R. Desiraju, *Acc. Chem. Res.* **2002**, *35*, 565.

[37] B. P. Finkenauer, Y. Gao, X. Wang, Y. Tian, Z. Wei, C. Zhu, D. J. Rokke, L. Jin, L. Meng, Y. Yang, L. Huang, K. Zhao, L. Dou, *Cell Rep. Phys. Sci.* **2021**, *2*, 100320.

[38] DOE Office of Energy Efficiency and Renewable Energy. Building Energy Codes Program: Prototype Building Models, https://www.energycodes.gov/prototype-building-models (accessed: September 2021).

[39] B. H. Toby, R. B. Von Dreele, *J. Appl. Crystallogr.* **2013**, *46*, 544.